ELSEVIER

Diamond and Related Materials 7 (1998) 1491–1502

DIAMOND AND RELATED MATERIALS

Growth of diamond films using an enclosed methyl-acetylene and propadiene combustion flame

K.L. Yarina [a,1], D.S. Dandy [a,*], E. Jensen [b,2], J.E. Butler [b]

[a] *Department of Chemical Engineering, Colorado State University, Fort Collins, CO 80523, USA*
[b] *Chemistry Division, US Naval Research Laboratory, Washington, DC, USA*

Received 20 November 1997; accepted 4 June 1998

Abstract

Diamond growth in low-pressure combustion flames was studied using a safer, more economical substitute for acetylene: a mixture of methylacetylene, propadiene, and liquefied petroleum (MAPP gas). A burner-stabilized, low pressure, flat, premixed flame was used to deposit continuous, uniform thickness diamond films on a heated molybdenum substrate. This work identifies the dependence of film growth rate and quality on the fuel-to-oxygen ratio and the burner–substrate separation distance at two different reactor pressures of 70 and 250 Torr. A single substrate temperature of 800 °C was used to consistently produce well-faceted films. For the MAPP/O_2 premixed flame, it was determined that the optimal fuel-to-oxygen ratios for diamond growth are 0.53 at 70 Torr and 0.51 at 250 Torr. Typical growth rates at these conditions were on the order of 1 μm h^{-1}. However, growth rate and quality are very sensitive to the fuel-to-oxygen ratio, falling off rapidly in either direction from the optimal value. Increasing the ratio enhances secondary nucleation, and eventually results in graphitic and amorphous material. The growth rate is also very sensitive to the burner–substrate separation distance due to tight coupling between the transport and chemical kinetic time scales in the combustion reactor.

Keywords: Combustion synthesis; Deposition; Diamond films; Morphology

1. Introduction

Combustion synthesis of diamond materials offers advantages not found in other methods of diamond chemical vapor deposition (CVD). First, at atmospheric pressure, the growth rates are still among the highest reported, over 100 μm h^{-1} [1]. Second, combustion CVD can produce high-quality diamond for use in optical and electronics applications because the presence of oxygen species improves the diamond quality by etching graphitic impurities up to 100 times more efficiently than atomic hydrogen; and where lattice damage by ionic species may be significantly lower than that found in plasma reactors [2]. Third, since combustion systems are highly convective by design, changes in feed gas composition rapidly affect the chemistry and resulting diamond films. By altering the feed gas composition during deposition in a cyclic fashion, the quality and rate of diamond growth can be controlled for the desired material properties [3–6]. In addition, installation of multiple burners for the coating complex shapes is potentially more straightforward in combustion systems than in other methods of diamond CVD.

Hirose and coworkers demonstrated the synthesis of polycrystalline diamond films using a common welder's torch [7,8]. They reported nominal growth rates of 200 μm h^{-1} for diamond particles and 100–150 μm h^{-1} for polycrystalline diamond films. More typically, however, Hirose et al. synthesized a semi-circular ring of diamond deposit using a fuel-to-oxygen ratio of 1.01–1.05, obtaining growth rates of 30 μm h^{-1} [9]. These initial results were soon confirmed by other investigators [10,11].

Acetylene–oxygen flames at sub-atmospheric pressures have been successfully used to deposit diamond over large areas [12–14], but with a drastic reduction in growth rate when compared to atmospheric pressure systems. Acetylene–oxygen diamond producing flat

* Corresponding author. Fax: +1 970 491 7369;
e-mail: dandy@engr.colostate.edu
[1]Present address: 3M Corporation, Bldg. 60-1N-01, St. Paul, MN 55144-1000, USA.
[2]Present address: Food and Drug Administration, HFS-246, 200 C Street SW, Washington, DC 20204, USA.

0925-9635/98/$ – see front matter
PII S0925-9635(98)00221-0

flames have been studied at pressures from 30 to 760 Torr. Uniform, polycrystalline diamond films have been observed over a 13-cm^2 area using a flat acetylene flame at 52 Torr [14]. At 30 Torr, observed growth rates are upwards of 2.3 μm h^{-1} over a 19-cm^2 area [13]. Other work at pressures of 40 Torr report uniform diamond films over at least a 2-cm^2 area with growth rates of 4 μm h^{-1} [15]. Recently, significant progress has been made in deposited highly textured ⟨100⟩ diamond films using bias-enhanced nucleation and low-pressure flat flames [16–18]. In those investigations, films were grown at a pressure of 47 Torr on 20-cm^2 (100) silicon substrates. Growth rates of up to 5.5 μm h^{-1} were measured, the highest recored low-pressure combustion growth rate at that time [16].

Alternatives to acetylene have also been examined under atmospheric and reduced pressure conditions. Initial studies of premixed oxygen–ethylene combustion focused on the use of brazing torches to explore the feasibility of this hydrocarbon source [19,20]. It was observed that, due to radial variations in the flame, the growth rate and nature of the deposit (diamond, a-C, graphite) varied with position on the substrate. Diamond crystallites were successfully grown at a fuel-to-oxygen ratio of 0.76. Later studies using low-pressure, flat premixed oxygen–ethylene flames resulted in continuous polycrystalline diamond films over 1.3 cm^2 on molybdenum substrates at a growth rate of 1.3 μm h^{-1} [21]. A propylene–oxygen premixed flat flame at 180 Torr was used to deposit diamond at a fuel-to-oxygen ratio of 0.47 [22]. This mixture corresponds to a C:O ratio of 0.70, which is considerably lower than the 1:1 C:O ratio required for acetylene–oxygen. This work suggests that non-equilibrium flame chemistry is important for diamond growth at low pressures [22]. Even the premixed methane–oxygen system, with its relatively low adiabatic flame temperature, has been used in a flat flame combustion reactor at 110 Torr to produce diamond at a rate of 0.2–0.3 μm h^{-1} [23].

MAPP is a cheaper alternative to acetylene and has been shown to produce diamond at low pressures [24]. MAPP gas is a mixture of approximately 56-wt% liquefied petroleum gas (mainly propylene), and 46% methylacetylene and propadiene, both isomers of C_3H_4. The cost of MAPP is roughly \$0.19 ft^{-3} or about 25% that of high-purity acetylene; additionally, MAPP has the advantage that it can be stored as a liquid. Liquid fuels are advantageous because they require less storage space than other hydrocarbons, such as acetylene, which must be stored as a gas. Harris et al. report diamond growth rates of approximately 1 μm h^{-1} from MAPP gas in a low-pressure combustion flame using fuel-to-oxygen ratios of 0.46 at 180 Torr and 0.51 at 70 Torr [24]. In that work, diamond growth was reported for only two conditions, and no determination was made regarding either the boundaries for diamond growth or the effect of changing parameters such as the fuel-to-oxygen ratio (R), the substrate temperature (T_s), or reactor pressure (p) upon the resulting diamond deposit. Further, no explanation was given as to why MAPP–oxygen flames must be more fuel-rich at lower pressures in order for diamond to grow, a result contrary to earlier findings with low-pressure acetylene [12] and ethylene flames [21,25].

The goal of the present work was to determine the boundaries of the diamond growth regime for a premixed, low pressure, flat flame using MAPP gas and oxygen. Also, the impact of changing processing conditions such as pressure and stoichiometry on the growth rate and quality of diamond were determined. The variability in the optical emission of the flame with operating conditions was examined for suitability as a real-time process monitor for use in combustion CVD of diamond.

2. Experimental

2.1. Apparatus

The combustion chamber used in this work consisted of a pair of 8-inch-diameter, stainless-steel crosses housing the torch feed from the bottom and the substrate feed from the top. On the chamber, there were three fused silica windows on 2.75-inch-diameter flanges that permitted optical access to the flame. The front port had a Pyrex window mounted on a hinged 8-inch-diameter door for viewing and access to the interior of the reactor. A schematic of the reactor setup is shown in Fig. 1. A more detailed view of the burner and substrate arrangement is shown in Fig. 2.

The torch body and nozzle were constructed of copper, and water cooled via a 0.25-inch copper tubing soft-soldered to the burner body. The burner body was a cylinder 1-inch deep, with a 0.75-inch inside diameter and a 1.5-inch outside diameter. The burner nozzle employed for the diamond growth in this work was a perforated design, which has been used previously for combustion synthesis of diamond [14,23]. The copper-perforated nozzle was 0.5 inches thick with 69 1-mm diameter holes arranged in a square array, with 1-mm spacing between the holes. This configuration resulted in a total cross-sectional area for flow of 0.542 cm^2. The 1-mm holes were large enough to prevent clogging from carbon deposits, during many hours of operation using a fuel-rich flame, and made the burner assembly easy to clean. The large solid surface area of the perforated nozzle gave a large surface for heat feedback from the flame and enhanced both the planarity and burner stabilization of the flame.

Premixed reactant gases entered the burner via a pair of opposing inlet ports at the bottom of the torch body,

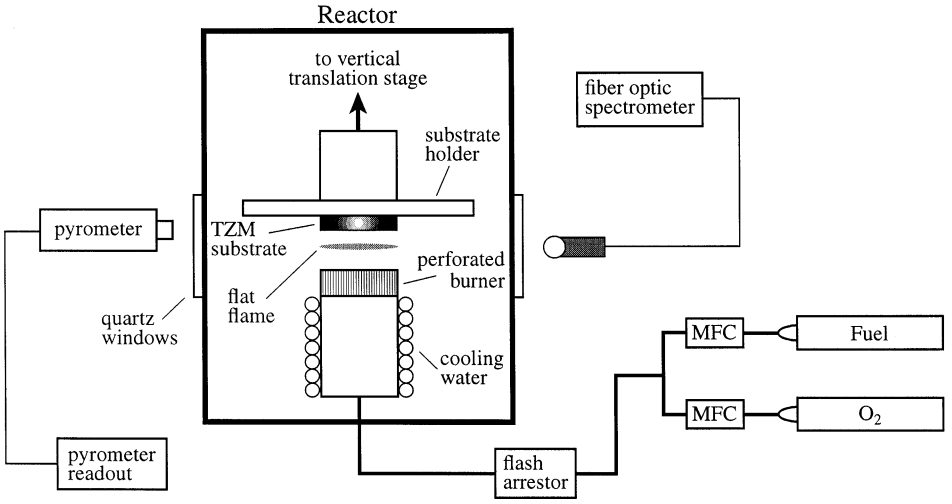

Fig. 1. Schematic of the low-pressure combustion reactor and equipment.

as illustrated in Fig. 2. The copper nozzle was attached to the top of the burner body, and one type C thermocouple to measure the temperature at the burner surface was inserted into a hole 2 mm outside the array of burner holes. High-temperature cement (Omega Eng.) held the thermocouple inside the hole drilled from the bottom of the burner. No thermocouple was placed in the center of the burner array because the wires interfered with the shape of the flame. Inlet and outlet burner cooling water temperatures were monitored by type K thermocouples (Omega Eng.) immersed in the flowing water and a microprocessor thermometer (Model HH23, Omega Eng.).

The substrate, positioned above the torch, was an 0.875-inch-diameter, 0.25-inch-thick tantalum–zirconium–molybdenum (TZM) alloy. This was held in place by a 3-inch stainless steel disk and three hex-head screws. Due to the low heat flux to the substrate from the low-pressure flame, it was necessary to heat the substrate externally with a removable 1-inch-diameter molybdenum cartridge heater (Spectramat) powered by a direct-current power supply (Sorensen, Model DCS 33-33). The substrate and heater were firmly held in direct thermal contact during the experiment using a clamping arrangement. The substrate temperature was measured by focusing a two-color (2.1- and 2.4-μm), infra-red optical pyrometer (Williamson, Model 8200), with operating limits of 700–1300 °C on the edge of the substrate. An X–Y–Z translation stage (Mitutoyo) enabled positioning of the entire substrate jig relative to the burner. A cathetometer (Eberbach) was positioned at a quartz window located 90° relative to the pyrometer. This device allowed a resolution of 0.1 mm in measuring the burner–substrate distance (D_s). The cathetometer also offered a convenient means of determining the degree to which the burner and substrate surfaces were parallel.

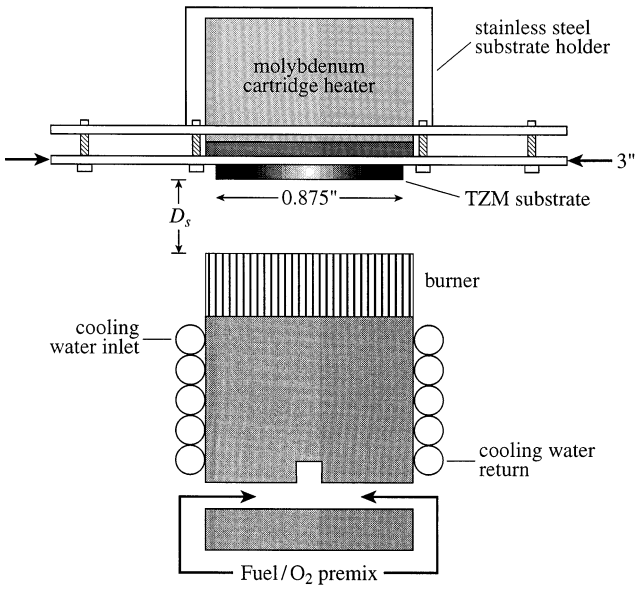

Fig. 2. Schematic of the burner/substrate configuration.

The hydrocarbon fuel and oxygen were supplied by gas cylinders and passed through mass flow controllers (MKS type 1159B). The mass flow controllers were controlled by a multigas PID controller (MKS Model 147B). The flow controllers were factory-calibrated and checked for accuracy in the laboratory and were determined to be accurate to 0.5% of full scale (10 slm). The reproducibility of the flow using these controllers was 0.2% of full scale, which corresponds to 0.02 slm. Thus, the error for the fuel-to-oxygen ratio, R, is ± 0.023 at 70 Torr where the total gas flow rate used was 2 slm. At 250 Torr, the total flow rate used was 4 slm, corresponding to an error in R of ± 0.011. A better reproducibility was observed at 250 Torr using a 4-slm total flow due to the proportionately smaller impact that the flow error had at larger flow rates.

A Stokes two-stage vane pump model V-023-2 rated at 55 cfm was connected to the chamber. A butterfly control valve (MKS Type 153) was in the line between the pump and the chamber. A capacitance manometer (MKS Type 107BA baratron) monitored the chamber pressure near the burner, and a PID controller (MKS type 146) was used to control the butterfly valve.

2.2. Diagnostics

A fiber-optic coupled CCD UV-vis spectrometer (Ocean Optics S1000) was used to monitor optical emission from the flame. The spectrometer detected wavelengths between 250 and 700 nm, and was used to monitor emission from C_2, CH, and OH species. The spectral response of the fiber-optic and CCD spectrometer was corrected using a calibrated tungsten lamp (Optronics Laboratories, Model 220M), which was supplied with NIST traceable points for a blackbody curve. A 35-mm single lens reflex camera was used for recording color photographs of the flame during deposition and the substrates after deposition.

The surface morphology of deposited films was analyzed using an optical microscope. A scanning electron microscope (SEM) was used for high-resolution imaging and to determine the size of the crystallites. Fourier-transform infra-red (FTIR) reflectance spectroscopy was employed to measure the thickness of the diamond films. The FTIR spectrometer provided the radiation source, detecting from 600 to 6000 cm^{-1}, and the light was reflected form the sample using a 30° angle of incidence. With this method, diamond film thickness was measured without removing the film from the substrate. The index of refraction for all deposited films was assumed to be that of diamond [26]. The thickness of the diamond film in the direction normal to the substrate surface was determined by

$$d = \frac{5000}{n_d \Delta v \cos\theta}\ (\mu m), \qquad (1)$$

where θ is the angle of incidence of the light, Δv (cm^{-1}) is the wavelength between the maxima of oscillation in reflected radiation, and $n_d = 2.4173$ is the refractive index of diamond.

Micro-Raman spectroscopy was used as a measure of the film quality. The Raman spectra were collected using the 514.5-nm argon ion laser line. The detector had a 3-cm^{-1} resolution from 505 to 1723 cm^{-1} with a focused spot size of the incident beam equal to 1–2 μm.

2.3. Growth conditions

The TZM substrate surface was prepared using wet (Sancap) or dry SiC sandpaper. Sanding removed previous carbon films or oxide layers, leaving a smooth, bare metal surface. Different grades of sandpaper were used: 220, 320, 400, and 600 grit. The final sandpaper used was always 600-grit SiC to obtain the smoothest possible finish.

To enhance nucleation rate and density, 0.1-μm diamond powder (type SJK-5 from Kay Industrial Diamond Corp.) was used to scratch the surface prior to deposition. The surface was seeded in order to provide reliable nucleation [27–29]. The substrate was polished for 2 min on a polishing plate impregnated with 0.1-μm diamond powder using a figure-of-eight pattern while rotating the substrate 90° every 30 s. Excess diamond powder was blown off the substrate using nitrogen.

Flame ignition took place once the reactor base pressure had stabilized to the set point and the substrate had been preheated to the desired temperature. Argon was used to flush the chamber and to raise the reactor pressure to the operating conditions while minimizing oxide formation on the hot substrate. The flame was ignited by simultaneously shutting off the argon flow while the fuel and oxygen were turned on, and momentarily generating an arc from a Tesla coil to the copper burner surface.

The duration of the deposition was monitored using a stopwatch and typically ranged from 1–5 h. Longer runs were not possible because soot formation on the substrate holder occluded the view of the edge of the substrate by the optical pyrometer. Runs were terminated when the substrate temperature could no longer be determined. After the desired length of time had passed, the fuel and oxygen flows were shut off simultaneously, and the control valve was opened, fully evacuating the chamber. The power to the substrate heater was shut off, and argon was passed through the burner, raising the reactor base pressure to 800 Torr. The substrate cooled at 800 Torr in an argon atmosphere for 1–2 h. The reactor was kept under a positive pressure during cool down, so that leaks did not allow oxygen into the chamber, thereby preventing oxidation of the deposit, substrate, and heater during cooling.

3. Results and discussion

3.1. Changing R

The stoichiometry of the flame, determined by the fuel-to-oxygen ratio, R, was varied to determine the values for which diamond was deposited. Subsequently, the deposited films were examined by SEM, FTIR, and Raman spectroscopy to determine the morphology, growth rate, and quality. A single substrate temperature was chosen for these experiments to reduce the number of variables. The effect of substrate temperature upon growth rate and quality in combustion flames was previously studied for atmospheric pressure flames [30]

and it was found that lower temperatures enabled broader ranges of R yielding diamond growth [31]. In addition, lower substrate temperatures have been observed to decrease carbon diffusion and carbide formation between the diamond film and metal substrate, resulting in easier delamination of diamond films. Applying these criteria, a substrate temperature of 800 °C was chosen as it yielded well-faceted polycrystalline films that could be easily removed from the substrate. Two operating pressures were chosen, 70 and 250 Torr, which were the low- and high-operating pressure limits of this reactor. Statistical design of experiments was not performed to optimize the growth rate or quality because an adequate metric of quality was not sufficiently well quantified by Raman spectroscopy due to the small number of data points [32]. Had more growth runs been carried out, such a technique may have been appropriate.

3.1.1. p = *70 Torr*

At 70 Torr, the effect of increasing the carbon content of the flame was examined by increasing R while keeping all other parameters constant, and these were $D_s = 7$ mm, $T_s = 800$ °C, and a total flow rate of 3.69 slm cm^{-2} of the burner area. Scanning electron micrographs of polycrystalline diamond films deposited over a 3-h period at $R = 0.504$, 0.527, and 0.550 are shown in Fig. 3a–c. These micrographs show the variation in morphology caused by increasing the carbon content in the flame. Clearly, the diamond film grown at $R = 0.527$, shown in Fig. 3b, exhibits the largest and most defined crystallites. This optimum value of R indicates that, although diamond grows over a range of R values, the central region produces the most crystalline diamond films.

Raman analysis indicates the presence of metal oxides and no evidence of diamond under fuel lean conditions. With extremely fuel-rich conditions, e.g. $R > 0.57$ at 70 Torr, the graphite bands at 1350 and 1580 cm^{-1} dominate the spectra, as illustrated in Fig. 4. Even under growth conditions that produce diamond films, it is difficult to use Raman as a judge of quality on these thin (several micrometers thick) films because the Raman intensity of diamond at 1332 cm^{-1} is directly proportional to thickness [33]. Consistent with the micrographs shown in Fig. 3, the Raman spectra in Fig. 4 indicate that the highest quality diamond is grown at $R = 0.527$.

3.1.2. p = *250 Torr*

Diamond films grown at a pressure of 250 Torr had a slightly higher growth rate than those grown at 70 Torr. Scanning electron micrographs are shown in Fig. 5a–c for films deposited at 250 Torr, with $D_s = 3$ mm, $T_s = 800$ °C, and a total gas flow rate of 7.38 slm cm^{-2} of the burner area, for different values of R, ranging from 0.49 to 0.55. The crystallinity of the deposit increases in the center of the diamond growing regime, as shown in Fig. 5b. Just as with diamond films grown at 70 Torr, the diamond crystals are the largest and most well defined in the center of the diamond growing regime, corresponding to $R = 0.510$ at this pressure. It should be noted that the diamond film shown in Fig. 5b was produced during a 4.5-h growth while Fig. 5a and c were produced during 3-h runs.

Raman spectra for the films grown at 250 Torr are shown in Fig. 6. These plots show the characteristic Raman peak for diamond films grown at $R = 0.510$ 0.493. However, the Raman signature for the sample grown at $R = 0.550$ clearly indicates a large number of defects, denoted by the broadness of the peaks, and primarily sp^2-bonded carbon, as indicated by the prominent peaks at 1350 and 1580 cm^{-1}. Thus, for MAPP gas, the optimal fuel-to-oxygen ratio for diamond film growth rate and quality appears to vary inversely with pressure, being optimized for diamond growth with $R =$ 0.527 at 70 Torr and $R = 0.510$ at 250 Torr.

3.2. Growth rate

As R is increased, the film growth rate increases, and the presence of broader Raman peaks at 1350 and 1580 cm^{-1} indicates more sp^2-bonded carbon content. The growth rate increased until the carbon deposit was primarily sp^2 carbon. At low R values, there was relatively more oxygen in the flame, and the substrate surface exhibited visible oxidation as a purple or orange substrate discoloration, and the Raman spectra showed oxides in the 700–900-cm^{-1} region.

The growth rate data for carbon films are shown in Fig. 7a for runs carried out at 70 Torr. The quoted growth rates assume linear growth and have been calculated by dividing the final film thickness by the total growth time. At 70 Torr, the maximum growth rate was approximately 1 μm h^{-1}. For the deposition runs at 250 Torr, the maximum growth rate was approximately 1.5 μm h^{-1} as shown in Fig. 7b. The reported growth rates are for carbon films in which both diamond and non-diamond carbon are present, as indicated by the Raman spectra in Figs. 4 and 6. The presence of non-diamond carbon contributes to an error in the prediction of the film thickness because the index of refraction in Eq. (1) was assumed to be that of diamond.

The increase in growth rate as the reactor pressure was raised from 70 to 250 Torr may be attributed primarily to the increase in inlet gas mass flow rates. The total gas flow was 2 slm at 70 Torr, and this quantity was raised to 4 slm at 250 Torr. It was not possible to operate with higher flow rates at 70 Torr because the flame would blow off the burner, and decreasing the flow rate at 250 Torr caused flashback into the burner. Because the diamond growth process is mass-transfer-limited, even under the reduced pressure conditions used

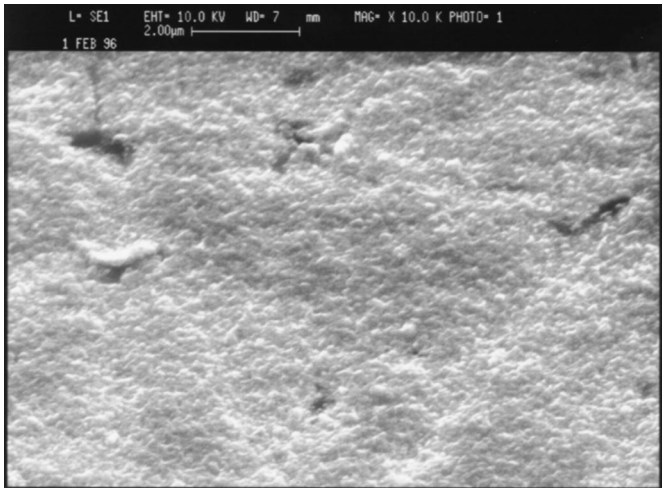

a

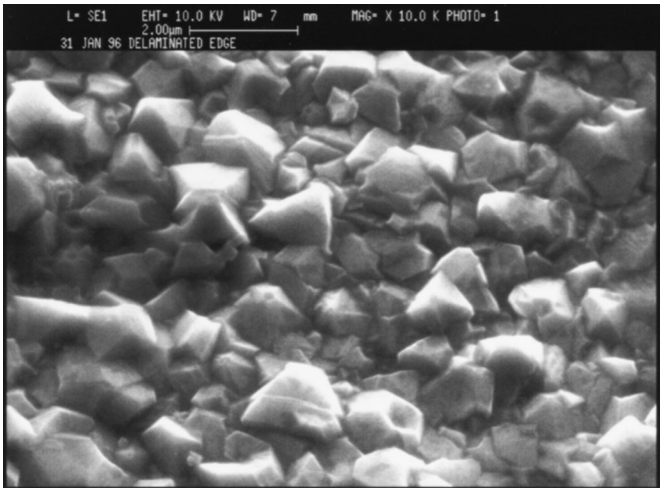

b

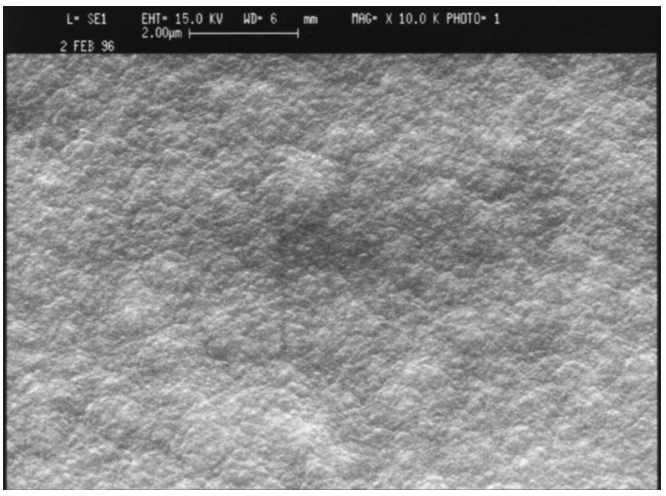

c

Fig. 3. Micrographs of diamond films deposited at 70 Torr and different fuel-to-oxygen ratios: (a) $R=0.504$; (b) $R=0.527$; (c) $R=0.550$. The film deposited at $R=0.527$ shows 1-μm-sized crystallites and the best faceting of any films grown at this pressure.

in this study [34], an increase in the gas flow rates results in an increase in deposition rate.

3.2.1. *Varying the burner to substrate distance, D_s*

Increasing the burner-to-substrate distance, D_s, resulted in a decrease in the rate of diamond deposition. Table 1 illustrates the decline in diamond growth rate with increasing D_s for experiments performed at 70 and 250 Torr, holding all other variables constant. These results indicate an extreme sensitivity of the growth conditions on the position of the substrate within the reacting gas flow. The highest growth rates were measured at the smallest values of D_s possible, 3 mm at 250 Torr and 7 mm at 250 Torr. These distances mark the closest possible substrate position without destabilizing or extinguishing the flame. The growth rate decreased monotonically with increasing D_s because of the increase in residence time of the gases before they reached the substrate. This increased time allowed the radical species that drive the deposition process (H, OH, hydrocarbon radicals, CH_3 in particular) to undergo gas-phase reactions to form stable, non-diamond-producing species [35]. The result is a decrease in the flux of diamond precursors to the substrate and decrease in the diamond growth rate.

3.3. *Optical emission*

Typical emission spectra from a premixed combustion flame used in this study are shown in Fig. 8. Three key species are present: OH A–X at 310 nm, CH A–X at 431.4 nm, and C_2 Swan (d–a) and Deslandres–d'Azambuja bands. Notably absent are H_α, H_β, and CN. The absence of CN emission suggests the absence of nitrogen, which is expected for an enclosed combustion flame with few leaks to the atmosphere. Visible emission from flames stems from chemiluminescent reactions and requires radical–radical interactions

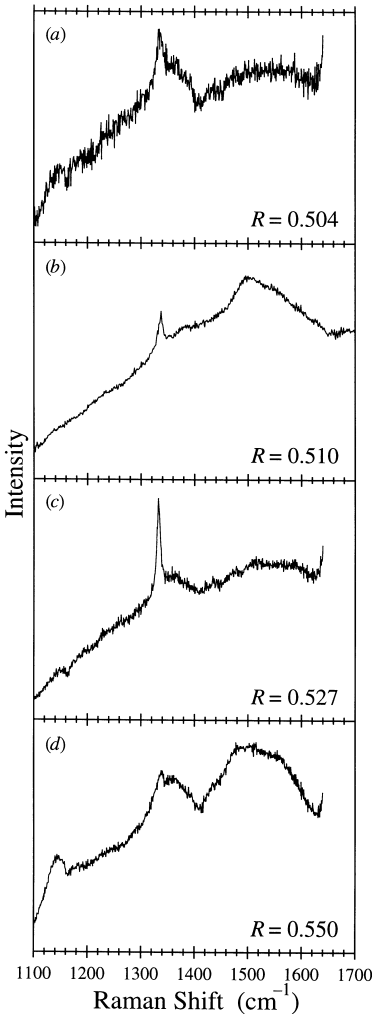

Fig. 4. Raman analyses of the films grown at 70 Torr indicate that the best quality diamond film was grown at $R=0.527$, in agreement with the SEM images displayed in Fig. 3.

[36]. In chemiluminescence, energetic species react to form electronically excited products in a flame. The spectra in Fig. 8 represent true chemiluminescence and explain why the intensity of optical emission from C_2 and CH species exceeds that expected from thermal excitation [36].

The relative emission intensities from OH, CH, and C_2 vary with pressure and R values. Spectra obtained at a constant pressure show a variation of intensity of the bands with R, as shown in Fig. 8. At the higher R value, 0.50, the C_2 swan bands are of a greater intensity than the CH band at 430 nm, and at the lower value, $R=0.40$, the CH emission is greater than that of the C_2 Swan bands. Since the ratio of C_2 to CH emission rapidly changes at these stoichiometries, this ratio is a good indicator of R in the flame. Optical emission is independent of errors in flow control and can be used as an independent metric to confirm R in the flame. Hence, the optical diagnostic may be used for real-time feedback of the process stoichiometry in combustion CVD of diamond.

Fig. 9 illustrates the pressure dependence of the emission ratio of the C_2 Swan band centered at 516 nm to the CH transition at 431 nm over a range of R values from 0.4 to 0.6. The gray and black boxes on the Fig. 9 indicate the approximate diamond growth regimes at 70 and 250 Torr, respectively.

3.4. Burner calorimetry

To model the gas phase chemistry accurately in a combustion system, the energy balance for the flame must be known. Energy may leave the flame via conduction into the burner and substrate surfaces in contact with the heated gas. Energy may also leave the flame via radiation losses to the surroundings. The remaining energy produced within the flame is then available to facilitate the combustion chemistry. The heat lost from the flame into the burner was calculated for several diamond producing runs at both 70 and 250 Torr, by measuring the temperature rise of the burner cooling water using thermocouple probes and the water flow rate using a volumetric flask and a stopwatch. The heat lost through the burner, Q, was determined using a simple thermodynamic relationship, $Q=\dot{m}C_p\Delta T$, where $\dot{m}$ is the mass flow rate of water (g s^{-1}), $C_p=4.18$ J/(g°C) is the heat capacity of water, and ΔT (°C) is the difference between the outlet and inlet cooling water temperatures. The heat lost to the burner for several diamond producing runs is shown in Table 2.

3.5. Temperature profile

A preliminary estimate of the flame temperature was measured using a fine wire thermocouple. The wire was inserted into the flame and the voltage across the thermocouple junction measured. An Omega type C, tungsten-5% rhenium/tungsten-26% rhenium, thermocouple with a 2320 °C melting point was used. The wires were 0.003 inches in diameter, with the diameter of the bare thermocouple junction equal to 0.25 mm. Type C thermocouples are not stable in the oxidizing environment of a flame. In this study, the bare thermocouple typically failed within 5 min due to rapid oxidation of the metal. To prevent oxidation and reduce radical recombination on the surface, a coating of high-temperature ceramic adhesive (Ceramabond 569) was used [37]. The coated thermocouple had a bead diameter of 0.5 mm.

The temperature measured by the thermocouple, T_c, differed from the actual gas temperature in the vicinity of the thermocouple, T_g, due to radiation losses from

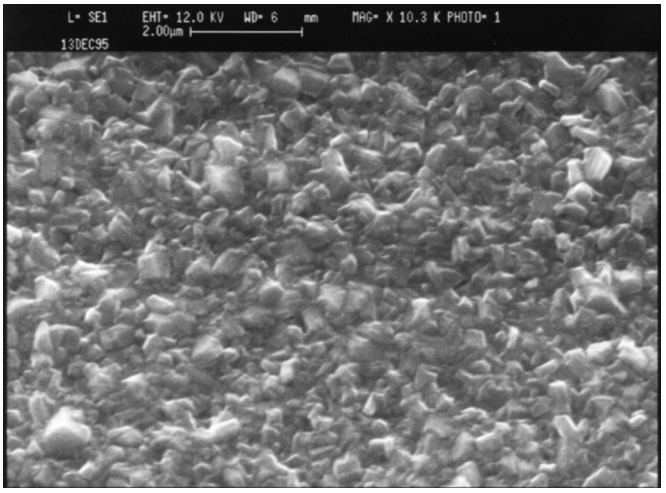

a

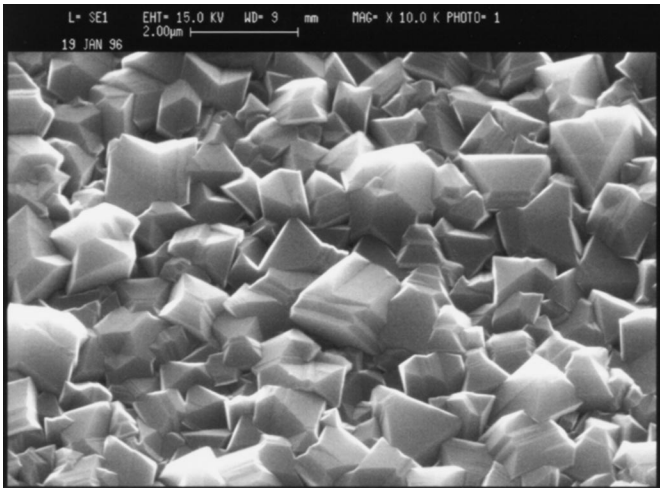

b

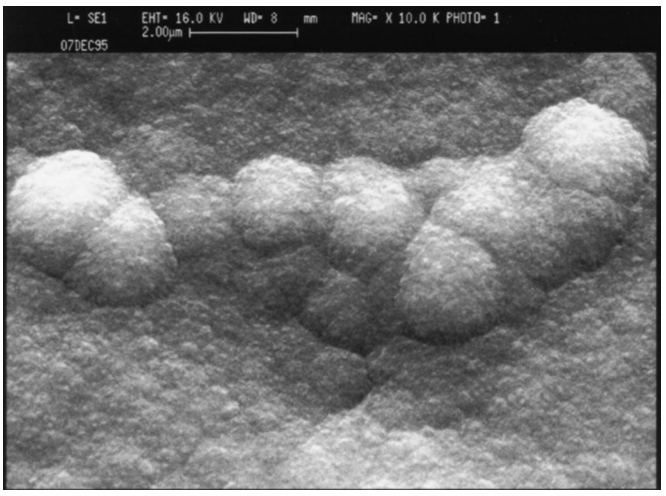

c

Fig. 5. Micrographs of diamond films deposited at 250 Torr and different fuel-to-oxygen ratios: (a) $R=0.493$; (b) $R=0.510$; (c) $R=0.550$. The film deposited at $R=0.510$ shows 2-μm-sized crystallites and the most well-defined crystals of any films grown at this pressure.

the thermocouple to its surroundings. An energy balance was applied to the thermocouple to obtain an expression for the necessary temperature correction. At steady state, the energy lost from the thermocouple by radiation to the surroundings and conduction along the wire is balanced by the energy gained by convective heating from the gas and catalytic recombination of atomic hydrogen on the thermocouple surface. In the experiments carried out, the thermocouple wire was placed nearly parallel to the flame isotherms such that conduction losses were small. Because the thermocouple was coated with a chemically inert ceramic, catalytic recombination had a negligible effect on energy gain. Thus, for gas flowing at a velocity u around a cylindrical bead of diameter d, the balance between convective heating of the thermocouple and radiation losses to the surroundings results in the following expression for temperature correction [36,38]:

$$T_g - T_c = \frac{1.25\epsilon\sigma d^{3/4}}{k}(v/u)^{1/4}[F_b(T_c^4 - T_b^4) + F_s(T_c^4 - T_s^4) + F_w(T_c^4 - T_w^4)]. \quad (2)$$

In this equation, k and v are the gas mixture thermal conductivity and kinematic viscosity, respectively, ϵ is the emissivity of the alumina bead coating (assumed to be 0.8), σ is the Stefan–Boltzmann constant, and F is the radiation view factor. Eq. (2) accounts for radiation exchange between the thermocouple and the burner surface (subscript b), the substrate (subscript s), and the reactor walls (subscript w).

The strategy for correcting the temperature using Eq. (2) was as follows. The physical properties of the gas were assumed to be that of an equimolar mixture

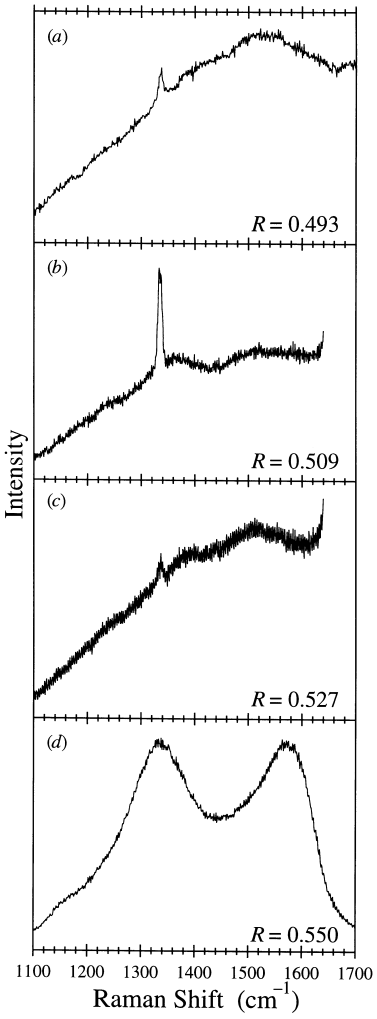

Fig. 6. Raman analyses of diamond films grown at 250 Torr indicate that the best quality diamond film was synthesized at $R=0.509$, whereas the spectra of the film produced at $R=0.550$ indicate non-diamond carbon with a high degree of disorder.

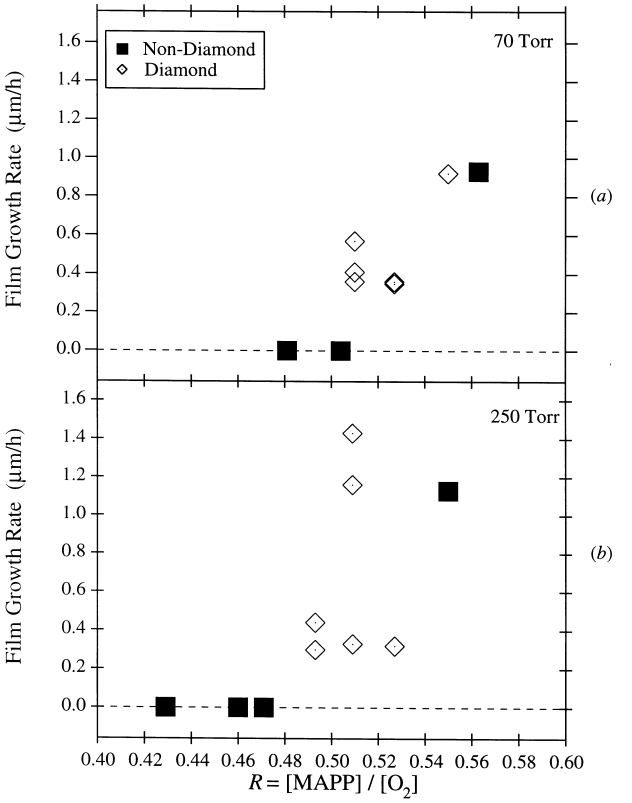

Fig. 7. Measured film growth rates at two reactor pressures, 70 and 250 Torr, for a substrate temperature $T_s=800$ °C. Closed squares indicate that no diamond 1332 cm^{-1} Raman peak was observed, and open symbols indicate that diamond was detected in the film. (a) 70 Torr, 2-slm total flow (1.5 slm for $R=0.510$), and burner–substrate separation $D_s=7$ mm ($D_s=7.5$ mm for $R=0.550$); (b) 250 Torr, 4-slm total flow, $D_s=3$ mm ($D_s=4$ mm for $R=0.527$).

Table 1
Effect of increasing separation distance (D_s) on growth rate

Pressure (Torr)	R=[fuel]/[O_2]	D_s (mm)	Growth rate (μm h^{-1})
70	0.510	7.0	0.49
		10.0	0.36
250	0.509	3.0	1.36
		4.0	0.20[a]
	0.527	3.0	0.32
		5.0	ND[a]
		5.8	ND[a]

[a]None detectable.

of carbon dioxide and water. The mixture thermal conductivity, k, was determined using the relation of Mason-Saxena [39], and the mixture kinematic viscosity, ν, was determined using the semi-empirical formula of Wilke [40]. The gas temperature correction was then calculated using the physical properties of this gas mixture at the thermocouple temperature, and then the gas correction was recalculated using the physical properties at this first estimate of the actual gas temperature. This process was iterated several times until the gas temperature converged to a single value. The criterion for convergence was 1 °C and usually occurred within the first three iterations. The radiation view factors also change with the position of the thermocouple. For each measured point of the temperature profile, the thermocouple position and temperature were used to calculate the temperature correction at that point.

The plot of corrected temperature profiles is shown in Fig. 10. When Fourier's law is applied to the profiles in this figure, the heat flux to the burner may be estimated as $-k(\Delta T/\Delta x)$, where k is the thermal conductivity of the gas mixture near the burner. The rate of heat transfer to the burner predicted via this approach is in quantitative agreement with the calorimetry measurements reported in Table 2, indicating that conduction is the dominant mechanism for heat transfer from the gas to the solid burner surface. The relatively flat temperature profile for the $R=0.55$ flame was due to the incipient failure of the thermocouple. In the flame,

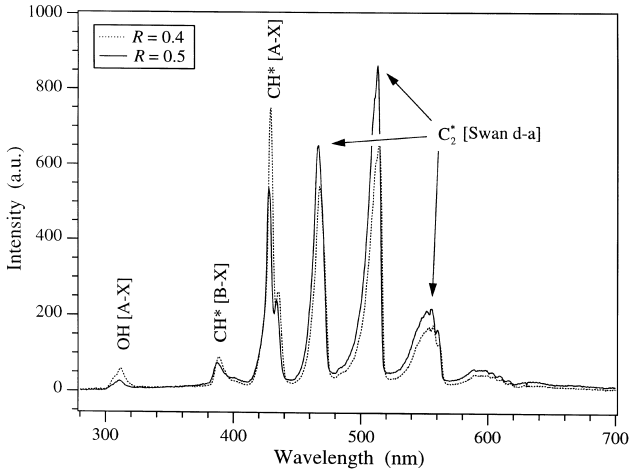

Fig. 8. Typical optical emission from a MAPP and oxygen premixed flat flame indicates the pressure sensitivity of the C_2^* Swan bands relative to the CH^* [A–X] transition at 430 nm. Optical emission may be useful as an independent indication of optimal diamond-producing fuel–oxygen mixtures.

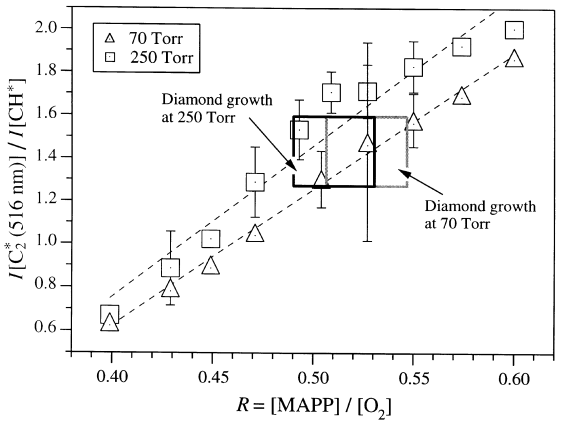

Fig. 9. Emission intensity ratios of C_2^*/CH at 70 and 250 Torr using the C_2^* peak at 516 nm.

even with the ceramic coating, the thermocouple did not have a very long lifetime, typically lasting only 1 h. Also, it is expected that the $R=0.51$ flame should be hotter than the $R=0.527$ flame, but this is contradicted by the results shown in Fig. 10. This counter-intuitive result may be due to the fact that the data for the $R=$

Table 2
The heat removed (Q) from the burner at temperature T_b during diamond growth as a function of the fuel-to-oxygen ratio, R

Pressure (Torr)	O_2 flow (slm)	MAPP flow (slm)	R	T_b (°C)	Q (W)
70	1.28	0.72	0.563	95	95.0
70	1.31	0.69	0.527	110	129.0
250	2.65	1.35	0.509	817	290.0
250	2.65	1.35	0.509	567	305.0
250	2.62	1.38	0.527	504	176.0
250	2.62	0.38	0.527	—	171.3

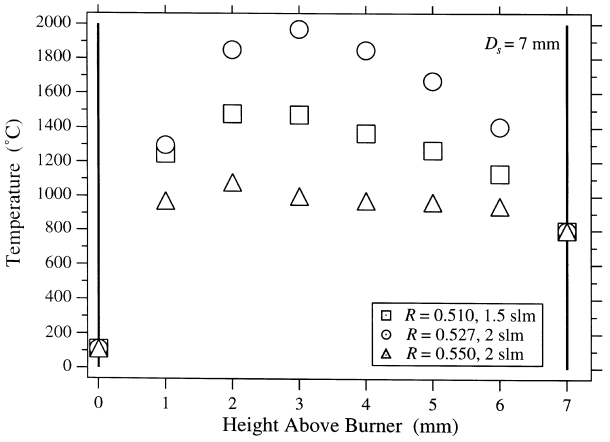

Fig. 10. Temperature profile of a diamond-producing flame using a fine wire thermocouple corrected for radiation losses. Operating conditions were 70 Torr pressure, 2-slm total flow, $D_s=7$ mm, and $T_s=800$ °C.

0.51 flame were taken at a total gas flow rate of 1.5 slm. The other data points were taken at a total flow rate of 2.0 slm. The different flow rates were selected to match the conditions at which diamond had been grown in earlier experiments.

The temperature profiles shown in this section are intended as data to assist in the modeling of the deposition process. Using the experimental temperature profile, a suitable reactor model will solve, using appropriate combustion mechanisms, for species concentration profiles through the flame. Such a combustion mechanism is not currently available for the C3 hydrocarbons used here, and it is beyond the scope of the present work to develop such a mechanism. Additionally, since energy transport near the substrate is dominated by conduction, the heat flux to the substrate may be calculated using Fourier's law by fitting a straight line through the temperature points, computing the slope of this line, and using the average gas mixture thermal conductivity.

4. Summary

A MAPP–oxygen premixed flat flame has been used to produce continuous, polycrystalline diamond films covering a 2.2-cm-diameter TZM alloy substrate. The conditions that yield diamond films in the MAPP–oxygen system have been characterized at the lower and upper operating limits of this flat flame burner, 70 and 250 Torr. The achievable growth rate and film quality (characterized by the Raman spectra) are comparable with existing low pressure acetylene–oxygen systems, and the results obtained here demonstrate that MAPP is a viable alternative to acetylene.

For the MAPP–oxygen premixed flame, the linear growth rate of continuous polycrystalline diamond films

was nominally 1 μm h^{-1}, occurring for $0.51 < R < 0.55$ at 70 Torr and $0.49 < R < 0.53$ at 250 Torr. These results for growth rate and fuel-to-oxygen ratio are consistent with an earlier study of the MAPP–oxygen system [24]. The slight shifting of the range of R resulting in diamond growth indicates a pressure dependence of the chemistry. This pressure dependence for MAPP–oxygen flames required more fuel-rich conditions as the pressure was reduced, a pattern apparently unique to this fuel. Comparatively, acetylene and ethylene combustion reactors require less carbon in the flame at reduced pressures to synthesize diamond. A detailed mechanistic investigation of the combustion kinetics for this fuel will be necessary before these observations can be explained. This inverse dependence of R on pressure is advantageous, however, because the present results indicate that high-quality diamond films can be deposited at higher growth rates by increasing the pressure and decreasing the amount of fuel.

The growth rate of diamond decreased sharply as D_s was increased past its optimum value of 3 mm at 250 Torr and 7 mm at 70 Torr. The rapid decrease in diamond growth rate was attributed to competing gas phase chemistry, which depleted the necessary diamond precursors in the gas phase before they reached the substrate. The extreme spatial dependence of radicals is unique to combustion systems and is less important in other highly convective systems, e.g. arcjets, where the concentrations of hydrocarbon species in the free stream are relatively constant until they reach the substrate and are depleted via surface reactions. Thus, D_s was observed to be an important parameter in combustion synthesis of diamond because of its influence on the formation of diamond and the film growth rate. The substrate must be positioned close to the flat flame, almost to the point of extinction, a distance that corresponds to the region just downstream of the bright luminescent portion of the flame, where radical species are at maximum concentration.

An explanation of the inverse behavior of MAPP–oxygen system at low pressure, that is, requiring more carbon in the flame to form diamond as the pressure was reduced, might be explained by careful analysis of the combustion mechanisms. Appropriate flame modeling could offer an explanation of the observed sensitivity of this geometry upon D_s. Unfortunately, current combustion mechanisms do not adequately predict the combustion products of MAPP or other C3 fuels. Thus, there is currently no satisfactory method of modeling the intermediate products formed in this combustion system at conditions that are observed to yield diamond.

A metric is proposed for combustion synthesis based on the ratio of C_2^* to CH^* emission intensity. The emission intensities of both species change rapidly near the R values which correspond to diamond growth and, hence, are a good indication of the region of diamond growth. Further, the C_2 swan band at 516 nm corresponding to the $\Delta v = 0$ transition must be used as opposed to the C_2 swan band at 467 nm corresponding to the $\Delta v = +1$ transition. Using this criterion, it was found that the emission ratio of C_2^*/CH^* had to be between 1.2 and 1.6 in order to facilitate diamond growth.

References

[1] K.V. Ravi, C.A. Koch, D. Olson, in: M. Yoshikawa (Ed.), 2nd Int. Conf. Applications of Diamond Films and Related Materials, MYU, Omiya, Japan, 1993, p. 491.
[2] D.E. Rosner, Annu. Rev. Mater. Sci. 2 (1972) 573.
[3] T.P. Thorpe, R.A. Weimer, J.A. Freitas, Appl. Phys. Lett. 65 (1994) 2490.
[4] J.A. von Windheim, F. Sivazlian, M.T. McClure, J.T. Glass, J.T. Prater, Diamond Relat. Mater. 2 (1993) 438.
[5] X.H. Wang, W. Zhu, J. von Windheim, J.T. Glass, J. Cryst. Growth 129 (1993) 45.
[6] R.A. Weimer, T.P. Thorpe, K.A. Snail, C.E. Merzbacher, Appl. Phys. Lett. 67 (1995) 1839.
[7] Y. Hirose, M. Mitsuizumi, New Diamond 4 (1988) 34.
[8] F. Akatsuka, Y. Hirose, K. Komaki, Jpn. J. Appl. Phys. 27 (1988) L1600.
[9] Y. Hirose, S. Amanuma, K. Komaki, J. Appl. Phys. 68 (1990) 6401.
[10] L.M. Hanssen, W.A. Carrington, J.E. Butler, K.A. Snail, Mater. Lett. 7 (1988) 289.
[11] L.M. Hanssen, W.A. Carrington, D.B. Oakes, J.E. Butler, K.A. Snail, in: R.E. Winans, R.G. Jenkins (Eds.), 197th American Chemical Society Meeting, Division of Fuel Chemistry, American Chemical Society, 1989, p. 444.
[12] N.G. Glumac, D.G. Goodwin, Thin Solid Films 212 (1992) 122.
[13] N.G. Glumac, H.S. Shin, D.G. Goodwin, Spring Technical Meeting of the Western States Section of the Combustion Institute, Combustion Institute, Davis, CA, 1994.
[14] N.G. Glumac, D.G. Goodwin, Mater. Lett. 18 (1993) 119.
[15] J.S. Kim, M.A. Cappelli, J. Mater. Res. 10 (1995) 149.
[16] C.A. Wolden, Z. Sitar, R.F. Davis, J.T. Prater, Appl. Phys. Lett. 69 (1996) 2258.
[17] C.A. Wolden, S.K. Han, M.T. McClure, Z. Sitar, J.T. Prater, Mater. Lett. 32 (1997) 9.
[18] C.A. Wolden, R.F. Davis, Z. Sitar, J. Mater. Res. 12 (1997) 2733.
[19] W.A. Carrington, L.M. Hanssen, K.A. Snail, D.B. Oakes, J.E. Butler, Metall. Trans. A 20 (1989) 1282.
[20] K.A. Snail, J. Macia, S. Kellogg, J.E. Butler, L.M. Hanssen, Carbon 28 (1990) 794.
[21] J.S. Kim, M.A. Cappelli, Appl. Phys. Lett. 65 (1994) 2786.
[22] H.S. Shin, D.G. Goodwin, Appl. Phys. Lett. 66 (1995) 2909.
[23] J.S. Kim, M.A. Cappelli, Appl. Phys. Lett. 67 (1995) 1081.
[24] S.J. Harris, H.S. Shin, D.G. Goodwin, Appl. Phys. Lett. 66 (1995) 891.
[25] K.A. Snail, D.B. Oakes, J.E. Butler, L.M. Hanssen, in: R. Messier, J.T. Glass, J.E. Butler, R. Roy (Eds.), New Diamond Science and Technology, Materials Research Society, Washington, DC, 1991, p. 503.
[26] R.C. Weast, CRC Handbook of Chemistry and Physics, CRC Press, Boca Raton, FL, 1995.
[27] N.G. Glumac, Ph.D. thesis, California Institute of Technology, Pasadena, CA, 1994.

[28] H. Liu, D.S. Dandy, Diamond Relat. Mater. 4 (1995) 1173.
[29] H. Liu, D.S. Dandy, Diamond Chemical Vapor Deposition: Nucleation and Early Growth Stages, Noyes Publications, Park Ridge, NJ, 1995.
[30] P.W. Morrison, A. Somashekhar, J.T. Glass, J.T. Prater, J. Appl. Phys. 78 (1995) 4144.
[31] L.M. Hanssen, K.A. Snail, W.A. Carrington, J.E. Butler, S. Kellogg, D.B. Oakes, Thin Solid Films 196 (1991) 271.
[32] W.A. Yarbrough, R. Messier, Science 247 (1990) 688.
[33] D.S. Knight, W.B. White, J. Mater. Res. 4 (1989) 385.
[34] D.S. Dandy, M.E. Coltrin, J. Mater. Res. 10 (1995) 1993.
[35] D.G. Goodwin, J.E. Butler, in: M. Prelas, G. Popovici, L.K. Bigelow (Eds.), Handbook of Industrial Diamonds and Diamond Films, Marcel Dekker, New York, 1997, p. 527.
[36] R.M. Fristrom, Flame Structure and Processes, Oxford University Press, New York, 1995.
[37] K.A. Burton, H.D. Ladouceur, J.W. Fleming, Combust. Sci. Technol. 81 (1992) 141.
[38] R. Siegel, J.R. Howell, Thermal Radiation Heat Transfer, Hemisphere Publishing, Washington, DC, 1992.
[39] R.H. Perry, C.H. Chilton, Chemical Engineer's Handbook, McGraw-Hill, New York, 1973.
[40] R.B. Bird, W.E. Stewart, E.N. Lightfoot, Transport Phenomena, Wiley, New York, 1960.